Analysis of Complex Cardiovascular Flow with Three Component Acceleration Encoded MRI

A. J. Barker[1], F. Staehle[1], J. Bock[1], B. A. Jung[1], and M. Markl[1]
[1]Medical Physics, Dept. of Radiology, University Medical Center Freiburg, Freiburg, Germany

Introduction: The assessment of in-vivo blood flow acceleration has the potential to provide valuable information regarding normal and deranged local flow characteristics (e.g. vortex flow with inherently high convective acceleration). Acceleration data may be estimated from standard velocity encoded images which, however, suffer from noise amplification when calculating spatiotemporal velocity derivatives [1]. Alternatively, the phase contrast (PC) principle can be employed to directly encode three-directional flow acceleration with tri-polar encoding gradients [2,3]. Thus, this study presents the *in-vitro* validation and *in-vivo* application of gradient optimized 2D PC-MRI designed to minimize TE and efficiently encode 3-directional, time-resolved acceleration [3,4]. In addition, 4D acceleration mapping at 3.0T is demonstrated in a healthy volunteer and an ascending aortic aneurysm patient. For all experiments, directly measured acceleration data were systematically compared to flow acceleration derived from velocity-encoded MRI. The combined visualization of velocity and acceleration data was performed to provide new insight into complex and pathologic flow phenomena. In addition, a simple contrast mechanism to visualize complex flow events such as boundary layer separation, turbulent reattachment, and vortex formation is presented.

Methods: For validation, a cylindrical stenosis phantom was used (Ø33.5±2.0 mm, max stenosis Ø10±0.1 mm; constant flow 5.9±0.5 L/min; blood-mimicking fluid 60:40 H_2O:glycerol). Experiments were performed on a 3T MR system (Trio, Siemens) using standard flow-sensitive 3D (venc=±150 cm/s; TE/TR=3.0/5.7ms) and acceleration sensitive 3D measurements (acceleration sensitivity, aenc=±150 cm/s^2; TE/TR=5.7/8.5 ms) with isotropic spatial resolution (1.0 mm^3). In 6 volunteers, *in-vivo* velocity and acceleration encoded 2D PC-MRI measurements of the left ventricular outflow tract were acquired [5]. Velocity encoding scans had an average scan length 5.5±1.4 min. (venc=±150 m/s; TE/TRs≈2.6/5.0 ms; spatial resolution=1.4x2.1x8 mm, temporal resolution Δt≈19.2ms). Acceleration-encoded 2D PC-MRI data were acquired with aenc=±50 m/s², TE/TR=7.4/10 ms, sequential encoding, and Δt=20 ms (same spatial resolution, average scan length 10.6±2.1 min) [3,4]. All scans were motion encoded in 3 principle directions. A central finite difference approximation was used to calculate the temporal and spatial acceleration from the flow-sensitive velocity measurements (referred to as 'velocity-derived acceleration') which were compared to the directly measured acceleration values (referred to as 'MR-measured acceleration'). A 4D velocity and acceleration scan of the thoracic cavity (voxel size≈2.0 mm^3, α=7°) was acquired in a healthy 29 year old male and a 26 year old male supracoronary aortic graft patient presenting a Ø5.0 cm ascending aortic aneurysm. (venc=±150 cm/s, TE/TR=2.5/5.1 ms, Δt=40.8 ms; aenc=±75 m/s^2, TE/TR=6.5/9.1 ms, Δt=72.8 ms). All *in-vivo* data were acquired during free breathing using prospective ECG and navigator gating.

Results and Discussion: Phantom experiments revealed substantially reduced noise in the MR-measured acceleration compared to the velocity-derived acceleration (Fig. 1c-d; noise, σ=1.3 versus 15.4 m/s^2) and improved accuracy (compared to theory, RMSE=2.6 versus 5.4 m/s^2). In addition, complex flow such as boundary layer separation (Fig. 1d, '*') and turbulent reattachment (Fig. 1d, '**') were clearly visible in the MR-measured acceleration images. Note that acceleration encoded magnitude images demonstrated enhanced intra-voxel dephasing due to complex flow, resulting in signal voids in regions with turbulence (Fig.1b, '**') [6]. Similar signal characteristics were found for in-vivo 2D acceleration mapping in the sinus of Valsalva and during aortic valve closure. These regions with signal loss were co-located with areas of high inertial (valve closure) or convective (vortex flow in sinuses) acceleration [5].

In-vivo acceleration waveforms correlated well between the two methods (ROI proximal to aortic valve: regression slope = 1.06, r^2=0.98, p<0.001). Similar to the phantom results, enhanced noise was consistently present in the velocity derived data as evident in Fig. 2a. Fig. 2b shows the concurrent visualization (Ensight, CEI, USA) of the volunteer results for the 4D velocity and 4D acceleration scans. The parallel alignment of the velocity and acceleration vectors at early and late systole indicate the presence of temporal acceleration (or deceleration, if antiparallel). For the majority of the cardiac cycle, the orthogonal velocity and acceleration vectors (Fig 2b, middle) indicate that convective acceleration was the dominant component contributing to the bulk acceleration. Similar results were observed in the 2D data. The combined visualization of 4D velocity and acceleration mapping in a aneurysm patient is presented in Fig. 3. As found in the 2D volunteer scans, regions seen to have highly vortical and disturbed flow, such as those in the ectatic portion of the arch (Fig. 3b) and those regions with secondary vortices and high velocity gradients (Fig. 3d), were co-located with signal loss (Fig 3c).

Conclusion: MR-measured acceleration was more accurate and significantly less noisy than velocity-derived acceleration. Vortex flow and boundary layer events were visible as higher order motion and lead to regions of signal loss, providing an easily recognizable marker for complex flow structure. The results from this work indicate that a combination of velocity and acceleration encoded data may improve the detection, visualization, and understanding of pathologic flow derangement.

Acknowledgements: DFG, Grant #MA 2383/4-1; BMBF, Grant #01EV0706; Whitaker & Fulbright Fellowships support AJB

References: **[1]** Balleux-Buyens, F, *et al.*, 2006, Phys. Med. Biol., Vol. 51, pp. 4747-58. **[2]** Tasu, JP, *et al.*, 2000, Magnet Reson Med, Vol. 44, pp. 66-72. **[3]** Staehle, F, *et al.*, 2009,ISMRM Abstract #2665. **[4]** Bernstein, MA, *et al.*, 1992, J Magn Reson Imaging, Vol. 2, pp. 583-8. **[5]** Staehle, F, *et al.*, 2010,ISMRM Abstract #70. **[6]** Gatenby, JC, *et al.*, 1993, Medical Physics, Vol. 20, pp. 1049-57.

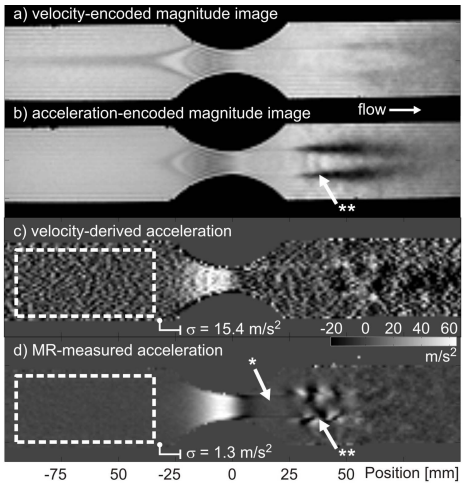

Fig.1. (a-b) Stenosis phantom magnitude images. **(c-d)** Velocity derived and MR-measured acceleration.

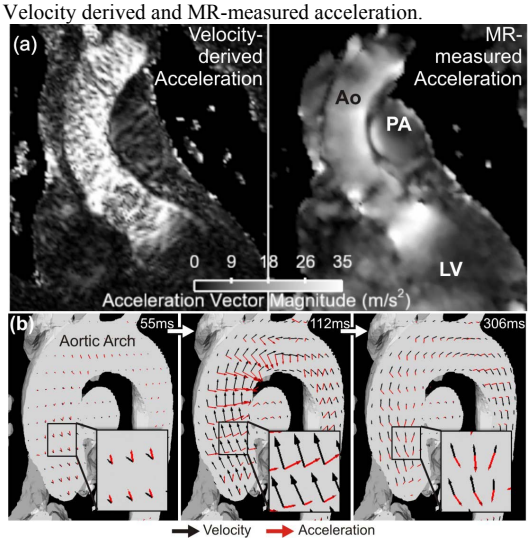

Fig.2. (a) 2D systolic acceleration maps. **(b)** Temporal evolution of velocity (black) and acceleration (red) vectors in a healthy volunteer 4D scan at early, mid, and end systole.

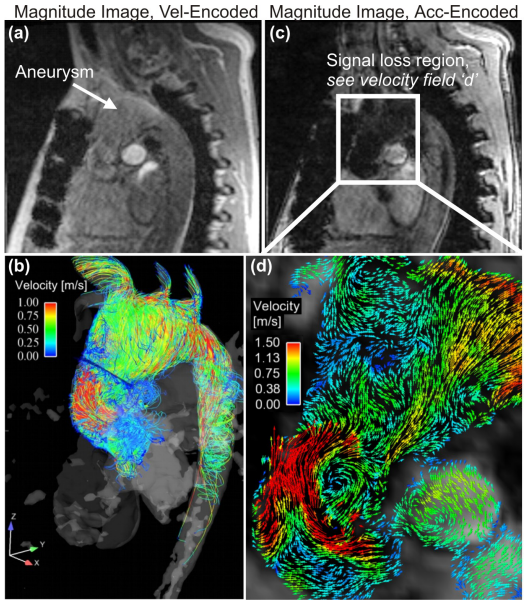

Fig.3. Complex aneurysm flow: **(a)** velocity magnitude image, **(b)** 4D velocity pathlines, **(c)** acceleration magnitude, & **(d)** velocity vectors overlaid on the acceleration magnitude image. →